



This is a repository copy of *Computational fluid dynamics and shape analysis enhance aneurysm rupture risk stratification*.

White Rose Research Online URL for this paper:

<https://eprints.whiterose.ac.uk/220364/>

Version: Published Version

Article:

Benemerito, I. orcid.org/0000-0002-4942-7852, Ewbank, F., Narracott, A. et al. (5 more authors) (2025) Computational fluid dynamics and shape analysis enhance aneurysm rupture risk stratification. *International Journal of Computer Assisted Radiology and Surgery*, 20 (1). pp. 31-41. ISSN 1861-6410

<https://doi.org/10.1007/s11548-024-03289-7>

Reuse

This article is distributed under the terms of the Creative Commons Attribution (CC BY) licence. This licence allows you to distribute, remix, tweak, and build upon the work, even commercially, as long as you credit the authors for the original work. More information and the full terms of the licence here:

<https://creativecommons.org/licenses/>

Takedown

If you consider content in White Rose Research Online to be in breach of UK law, please notify us by emailing eprints@whiterose.ac.uk including the URL of the record and the reason for the withdrawal request.



eprints@whiterose.ac.uk
<https://eprints.whiterose.ac.uk/>



Computational fluid dynamics and shape analysis enhance aneurysm rupture risk stratification

Ivan Benemerito^{1,2} · Frederick Ewbank³ · Andrew Narracott^{1,4} · Maria-Cruz Villa-Uriol^{1,5} · Ana Paula Narata⁶ · Umang Patel⁷ · Diederik Bulters³ · Alberto Marzo^{1,2}

Received: 24 July 2024 / Accepted: 30 October 2024
© The Author(s) 2024

Abstract

Purpose Accurately quantifying the rupture risk of unruptured intracranial aneurysms (UIAs) is crucial for guiding treatment decisions and remains an unmet clinical challenge. Computational Flow Dynamics and morphological measurements have been shown to differ between ruptured and unruptured aneurysms. It is not clear if these provide any additional information above routinely available clinical observations or not. Therefore, this study investigates whether incorporating image-derived features into the established PHASES score can improve the classification of aneurysm rupture status.

Methods A cross-sectional dataset of 170 patients (78 with ruptured aneurysm) was used. Computational fluid dynamics (CFD) and shape analysis were performed on patients' images to extract additional features. These derived features were combined with PHASES variables to develop five ridge constrained logistic regression models for classifying the aneurysm rupture status. Correlation analysis and principal component analysis were employed for image-derived feature reduction. The dataset was split into training and validation subsets, and a ten-fold cross validation strategy with grid search optimisation and bootstrap resampling was adopted for determining the models' coefficients. Models' performances were evaluated using the area under the receiver operating characteristic curve (AUC).

Results The logistic regression model based solely on PHASES achieved AUC of 0.63. All models incorporating derived features from CFD and shape analysis demonstrated improved performance, reaching an AUC of 0.71. Non-sphericity index (shape variable) and maximum oscillatory shear index (CFD variable) were the strongest predictors of a ruptured status.

Conclusion This study demonstrates the benefits of integrating image-based fluid dynamics and shape analysis with clinical data for improving the classification accuracy of aneurysm rupture status. Further evaluation using longitudinal data is needed to assess the potential for clinical integration.

Keywords Aneurysm · Fluid dynamics · PHASES · Logistic regression · Risk factors · Shape

Introduction

The management of patients with unruptured intracranial aneurysms (UIA) remains a clinical challenge. While 3% of adults have one, only a small percentage of these rupture [1]. When they do rupture, they cause subarachnoid haemorrhage, which results in significant morbidity and mortality [2].

Currently, the only options for prophylactic treatment are endovascular and surgical interventions [2]. Despite advances in these approaches, they remain associated with

✉ Ivan Benemerito
i.benemerito@sheffield.ac.uk

¹ INSIGNEO Institute for in Silico Medicine, University of Sheffield, Sheffield, UK

² Department of Mechanical Engineering, University of Sheffield, Sheffield, UK

³ Department of Neurosurgery, University Hospital Southampton, Southampton, UK

⁴ Division of Clinical Medicine, University of Sheffield, Sheffield, UK

⁵ Department of Computer Science, University of Sheffield, Sheffield, UK

⁶ Department of Neuroradiology, University Hospital Southampton, Southampton, UK

⁷ Department of Neurosurgery, Oxford University Hospital NHS Foundation Trust, Oxford, UK

complication rates ranging from 3 to 10% [3, 4]. Subsequently, in clinical practice, the decision on whether to treat an aneurysm relies on comparing the perceived risk of its rupture against the risks associated with its treatment. In recent years, a number of natural history studies have investigated factors associated with aneurysm rupture. The standard risk stratification model for estimating the risk of rupture is the PHASES score [5], which uses six clinical variables (ethnicity, hypertension, age, aneurysm size, aneurysm location, history of previous SAH) to estimate the five-year risk. While this scoring system achieved an AUC (Area Under the Curve, ROC) of 0.82 on its original dataset, its performance deteriorates when applied to external data [6–8].

Although the best available model, the PHASES score remains a crude assessment of the risk of rupture and there remains a need for more detailed and personalised risk estimates. Angiographic imaging and derived haemodynamic and morphological data hold vast potential. In recent years, the development of computational fluid dynamics (CFD) has provided insight into aneurysm rupture, with factors like wall shear stress [9], oscillatory shear index [10] and residence time [11] already explored. This has led to the understanding that aneurysms with irregular shapes (e.g. high aspect ratio [12] or presence of bulges [13]) or that exhibit complex flow patterns [14] are more prone to rupture, and identification of novel risk factors derived from shape and haemodynamic analyses. These factors have been integrated into several rupture classification models [14–17], although none has been implemented in clinical practice. One reason for this is that CFD and morphology models have not been tested to see if they add any predictive value over and above routinely available clinical variables. To improve their clinical uptake, it is also necessary to reduce their lengthy processing, feature-extraction, and evaluation times, to show that the feature extraction operation can be performed repeatably and reliably, and to show that the adoption of computer-derived data is beneficial in a clinical context.

This study's first aim is to evaluate whether haemodynamic and morphological data generated within the pipeline developed as part of the European project @neurIST [18], can improve the distinction between ruptured and unruptured aneurysms compared to the PHASES score. Its second aim is to identify which image-derived features of aneurysm shape and flow most strongly correlate with rupture status in order to optimise the feature set and facilitating integration of computational risk models with existing clinical workflows.

Methods

Patient population

Patient data was collected within the European Union funded @neurIST project (FP6-IST). In this study patients were recruited from seven clinical centres across Europe (UK, Switzerland, Hungary, Netherlands, Spain, and Ireland). Ethical approval and patient consent were obtained for all patients according to local ethics and data usage regulations. All images and patient data were processed exclusively within the @neurIST project.

The @neurIST project recruited over 1400 participants. However, only those with both 3D Rotational Angiographies (3DRA) and complete PHASES data were included for analysis and processed to obtain patient-specific morphological and haemodynamic data. This resulted in a final study population of 170 patients, divided into 78 with ruptured aneurysms and 92 with unruptured aneurysms.

The representativeness of the dataset was tested by comparing the distributions of demographic and aneurysm characteristics with those in the PHASES study, which also includes the UCAS and ISUIA studies and amounted to 8382 participants [5]. These are shown in Table 1.

Unlike the dataset from the PHASES study, the @neurIST dataset presents a relatively balanced split between ruptured and unruptured cases. Furthermore, the distribution of patients between ruptured and unruptured cases differs for the two datasets for key features such as hypertension and previous SAH, as well as for all age groups except those younger than 40 years. Because of the different distributions between PHASES and @neurIST, as well as the fact that the PHASES score was developed from longitudinal data, while our dataset is of cross-sectional nature, in building the logistic regression models we decided not to use the aggregate score of the six PHASES variables as originally developed in [5], but rather treated the PHASES variables as individual and independent features. Further details are provided in the Additional Material.

Morphological and haemodynamics analysis

The @aneurIST toolchain, described in detail in [19], was employed to segment all 3DRA images, allowing for the extraction of the specific geometry for each individual aneurysm. Segmented geometries were meshed to run a computational fluid dynamics (CFD) analysis of the blood flow within the aneurysm and in the surrounding regions. A full cardiac cycle was simulated: inlet conditions were imposed as a flow-rate waveform, whereas outlet conditions were represented using a pressure waveform. Flow-rate and pressure waveforms were computed with a generic whole body 1D circulation model set-up within the @neurIST toolchain [20].

Table 1 Comparison of demographic and aneurysm characteristics between PHASES and @neurIST datasets

	PHASES		@neurIST dataset	
	Rupture ($n = 220$) (%)	No rupture ($n = 8162$) (%)	Rupture ($n = 78$) (%)	No rupture ($n = 92$) (%)
Patient characteristics				
<i>Women</i>	74	68	72	74
<i>Age</i>				
< 40 years	12	5	12	9
40–49 years	11	13	33	33
50–59 years	16	28	38	39
60–69 years	25	33	12	16
≥ 70 years	37	24	8	4
<i>Hypertension</i>	53	44	27	44
<i>Previous SAH</i>	23	13	6	4
Aneurysm characteristics				
<i>Size at the time of detection</i>				
< 5.0 mm	26	48	70	35
5.0–6.9 mm	13	26	20	31
7.0–9.9 mm	18	15	21	27
10.0–19.9 mm	29	11	7	4
≥ 20 mm	17	2	3	0
<i>Location</i>				
ICA	38	38	18	42
MCA	25	34	27	23
ACA/PCA	38	29	56	36

Medical images and segmented geometries were processed to extract the patient-specific morphological features of the aneurysm. While the toolchain aimed for automation, the evaluation of certain morphological variables such as the location of the aneurysm neck (which must be identified through manual landmarking) and the aspect ratio required human intervention. Guidelines were provided to ensure consistency of these subjective variables. Similarly, relevant haemodynamic variables were determined by post-processing the results of the CFD simulations. This yielded the morphological (shape) and haemodynamic (CFD) variables shown in Table 2. As explained in the next section, only a subset of the variables shown in Table 2 are included in the final model.

Classification models

To assess the potential of image-based computed data in improving the classification of aneurysm rupture compared to using PHASES alone, five logistic regression models were constructed (Table 3). The reference model (P) included only PHASES variables. The remaining models evaluated the contribution of additional data:

- Model PC combined PHASES with CFD-derived features
- Model PS combined PHASES with shape-derived features
- Model PCS incorporated both CFD and shape features along with PHASES variables.
- Model CS solely relied on CFD and shape features, excluding PHASES.

Feature reduction: correlation coefficient and principal component analysis

To prevent issues arising from multicollinearity of the input variables, we reduced the dimensionality of the C (CFD-derived) and S (shape-derived) features before training the classification model. We aimed at retaining all the PHASES variables in all models. However, we excluded ethnicity due to a lack of variability as the dataset included no patients from Finland or Japan. Additionally, the size of the aneurysm (AneuDepth) obtained from the @neurIST toolchain was treated as a PHASES variable, not as an S variable.

Lasso optimisation has been previously used in the literature for automatic feature reduction of logistic regression models [15, 21]. However, preliminary investigation of the

Table 2 Complete list of morphological and haemodynamics variables with their definition, before the highly correlated features are removed from the analysis

Feature	Definition	Type	Units	Assessment
AR	Aspect ratio	Shape	Adimensional	Manual
NWidth	Diameter of aneurysm neck	Shape	m	Manual
Surface	Aneurysm surface	Shape	m ²	Automatic
NSurf	Surface area of aneurysm neck	Shape	m ²	Automatic
Vol	Aneurysm volume	Shape	m ³	Automatic
NSI	Non-sphericity index	Shape	Adimensional	Automatic
AbsHighWSSAreaAvg	Area of high WSS, average over time within aneurysm	CFD	m ²	Automatic
AbsLowWSSAreaAvg	Time average of low WSS area within aneurysm	CFD	m ²	Automatic
RelHighWSSAvg	Percentage of high WSS area, averaged over time within aneurysm	CFD	Adimensional	Automatic
RelLowWSSAreaAvg	Percentage of aneurysm area with low WSS, averaged over time	CFD	Adimensional	Automatic
AbsHighWSSAreaPeak	Area of high WSS at peak systole within aneurysm	CFD	m ²	Automatic
RelHighWSSPeak	Percentage of aneurysm area with high WSS at peak systole	CFD	Adimensional	Automatic
MaxWSSPeak	Maximum WSS at peak systole	CFD	Pa	Automatic
AbsHighOSIArea	Area of elevated OSI within aneurysm	CFD	m ²	Automatic
RelHighOSIArea	Percentage of area with high OSI within aneurysm	CFD	Adimensional	Automatic
MaxOSI	Maximum oscillatory shear index within aneurysm	CFD	Pa	Automatic
AbsHighPAreaPeak	Area of high pressure at peak systole within aneurysm	CFD	m ²	Automatic
RelHighPAreaPeak	Percentage of aneurysm surface with high pressure at peak systole	CFD	Adimensional	Automatic
MaxPPeak	Maximum pressure at peak systole within aneurysm	CFD	Pa	Automatic
AvgVAvg	Average velocity inside aneurysm, averaged over time	CFD	m/s	Automatic
AvgVPeak	Average velocity inside aneurysm at peak systole	CFD	m/s	Automatic
MaxVAvg	Time average of maximum velocity inside the aneurysm	CFD	m/s	Automatic
MaxVPeak	Maximum velocity in aneurysm at peak systole	CFD	m/s	Automatic
MaxVNPeak	Maximum velocity in aneurysm neck at peak systole	CFD	m/s	Automatic
MaxFluxNeck	Maximum flux through aneurysm neck	CFD	kg*m/s	Automatic
MomFluxPeak	Momentum flux through aneurysm neck at peak systole	CFD	kg*m/s	Automatic
AbsInfluxAreaPeak	Area of influx flow into the aneurysm at peak systole	CFD	m ²	Automatic
RelInfluxAreaPeak	Percentage of neck area with influx flow into aneurysm at peak systole	CFD	Adimensional	Automatic
VisDis	Viscous dissipation within aneurysm	CFD	W	Automatic

Table 3 Number of variables after feature reduction, including the dummy variables used for the categorical features

Feature group	Initial number of features	Number of features when threshold = 0.7	Number of features when threshold = 0.8	Number of features when threshold = 0.9
P	6	6	6	6
PC	30	20	23	27
PS	12	9	10	10
PCS	36	23	27	31
CS	30	17	21	25

dataset using lasso regression resulted in a feature pool that did not include any PHASES variables, thus violating our initial aim. Attempts to force the inclusion of PHASES variables within the final model by modifying the penalty term in the cost function proved not effective. Thus, we performed feature reduction using two distinct methods [22, 23], and then used the reduced feature set for ridge logistic regression [24]:

- I. Pearson correlation coefficient to identify features with high correlation, potentially indicating redundancy.
- II. Principal Component Analysis (PCA) to create a new set of uncorrelated features that capture most of the information in the original data.

For the correlation-based method, we removed features with Pearson correlation coefficients exceeding a specific threshold, ranging from 0.7 to 0.9, and that reached significance level ($p < 0.01$). The resulting models (P, PS, PC, PCS, and CS) and the number of features used in each are shown in Table 3.

For the PCA-based method, we computed the principal components of the CFD and shape variables separately, and then combined them with the PHASES variables to obtain the PCA-derived P, PS, PC, PCS, CS models. PCA analysis was performed using the Python3 package Sklearn, version 1.3 [25].

Logistic regression models

For both correlation-based and PCA-based models, the same statistical modelling procedure was used. All the numerical variables were treated as continuous variables and standardised by subtracting their standard deviation and dividing by their mean values. Categorical variables from PHASES were included as dummy variables. We used ridge logistic regression [24], implemented in Sklearn, for classifying ruptured and unruptured aneurysms [14, 15, 21]. Logistic regression computes the probability $p(\mathbf{x})$ that an event occurs, in this case an aneurysm belonging to the ruptured group, given a set of n parameters $\mathbf{x} = \{x_1, \dots, x_n\}$ and the set of coefficients $\boldsymbol{\beta} = \{\beta_0, \beta_1, \dots, \beta_n\}$. This is done through the logistic regression equation:

$$p(x) = \frac{1}{1 + e^{-(\beta_0 + \beta_1 x_1 + \dots + \beta_n x_n)}} \quad (1)$$

Each parameter x_i represent a PHASES, CFD or shape variable. The coefficients β_i indicate the weight of the parameter x_i in determining the probability $p(\mathbf{x})$ and are computed through model fitting. For the purpose of model fitting, we used eighty percent of the dataset for training and the remaining twenty percent for testing. We randomised the splitting

Table 4 Performance of the logistic regression models. Since PHASES variables are never removed, results for correlation-based and PCA-based logistic regression models are the same

Feature group	Correlation based	PCA based
P	0.64 ± 0.08	
PS	0.69 ± 0.08	0.66 ± 0.09
PC	0.71 ± 0.08	0.69 ± 0.08
PCS	0.71 ± 0.08	0.68 ± 0.08
CS	0.71 ± 0.08	0.69 ± 0.08

by performing ten-fold cross validation. Within each fold we optimised the ridge regularisation parameters and the model coefficients through a grid search algorithm under the constraint that the AUC of the resulting ROC was maximised. This procedure of randomised splitting and optimisation was repeated with 500 iterations of bootstrap resampling to compute the confidence intervals of the model coefficients [15]. The best performing model, that is the model that showed the highest AUC during training, was then evaluated on the test dataset. Since we designed the logistic regression to predict the probability that patients belong to the ruptured group, a positive coefficient β_i means that the feature x_i is associated with membership to the ruptured group.

Results

Feature reduction: Pearson's correlation

As shown in Table 3, the number of variables retained in the model changed with the correlation threshold: an increase in the threshold reduced the number of variables that were filtered out, thus leading to models that require more parameters. The list of features retained in each group for a correlation threshold 0.7 are shown in Table 5.

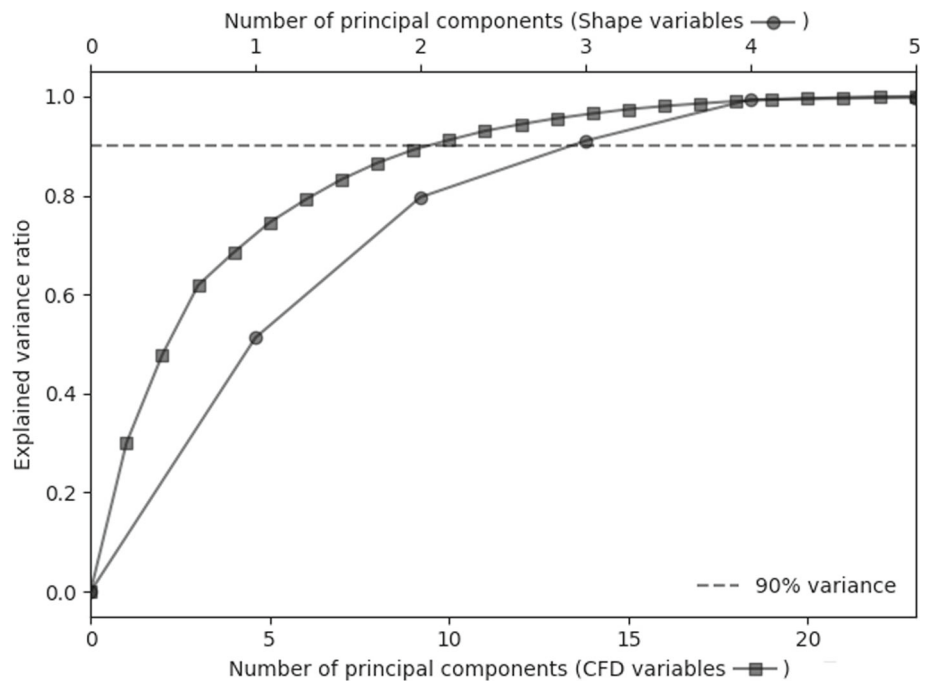
Feature reduction: PCA

The amount of variance explained by the principal components of CFD-derived and morphological features is shown in Fig. 1. In what follows, we will present the results of the logistic regression models built with ten components for CFD variables and three for shape features, that were able to explain 90% of the variance of the original features.

Classification models

Changing the correlation threshold in the feature reduction approach using Pearson's correlation had only a minor effect, thus we show in Table 4 only the results obtained when such

Fig. 1 Percentage of explained variance as a function of the number of principal components for haemodynamics and morphological features



threshold was set to 0.7. When the correlation-based feature reduction method is adopted, using only PHASES variables produced the lowest AUC values, with mean \pm standard deviation $AUC = 0.636 \pm 0.084$. The inclusion of shape data increased the AUC to 69.2 ± 7.9 . Inclusion of CFD variables also improved prediction, with $AUC = 0.71 \pm 0.085$ for the PC group. Further addition of both CFD and shape variables did not further improve classification in the PCS model ($AUC = 0.709 \pm 0.084$). The use of derived data alone (group CS) yielded an $AUC = 0.709 \pm 0.084$. The corresponding average ROC curves are shown in Fig. 2.

Results from using logistic regression models after PCA-based model reduction are consistent and show similar performance.

Table 5 presents the average value and 95% confidence intervals for the coefficients of the best logistic regression models for each group, after the feature reduction with correlation threshold 0.7. As explained above, positive sign of the coefficient means that the corresponding feature is associated with ruptured status. Most of the features tend to be associated with only state, either ruptured or unruptured. The only exceptions are represented by Age, AneuDepth and RelLowWSSAreaAvg. Results from logistic regression on the P group identify both Age and AneuDepth as indicative of rupture status. They are however evaluated as characteristic of unruptured status in groups PC, PS and PCS. Similar behaviour is observed for RelLowWSSAreaAvg, which appears to be associated with rupture in PC and with unruptured in PCS and CS. NSI and MaxOSI are the variables that are most strongly associated with rupture and show

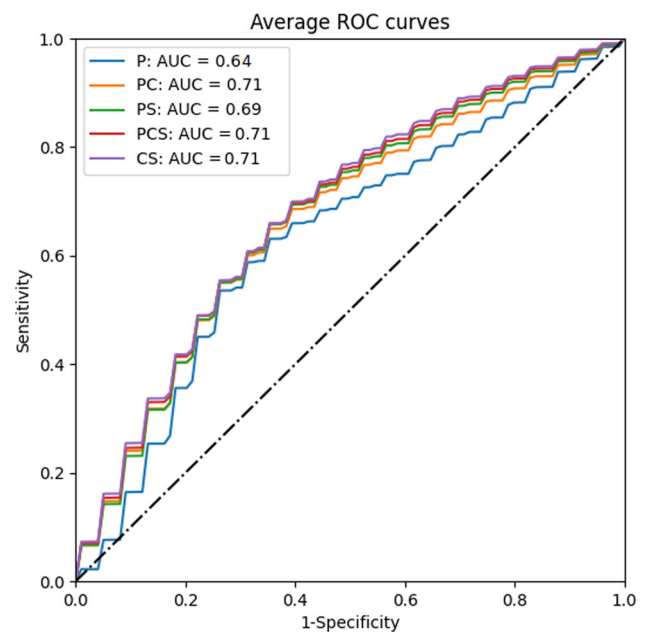


Fig. 2 Average ROC curves for the five correlation-based logistic regression models. The ROC curves for each group are obtained using the variables that are retained after the correlation-based feature reduction. The feature for each group are listed in the corresponding column of Table 3

narrow 95% confidence intervals. This is true for all the groups where these variables are included, in which they consistently rank high. In agreement with this, patients where large areas of the aneurysm are subject to high OSI are more likely to suffer a rupture (variable RelHighOSIArea). Likewise, rupture is associated with low wall shear stresses

Table 5 coefficients of the final logistic regression models (correlation threshold: 0.7) of the five groups with the 95% confidence interval reported in brackets

Feature	P	PC	PS	PCS	CS
Age *	0.009 [0.002; 0.017]	- 0.013 [- 0.015; - 0.01]	- 0.023 [- 0.031; - 0.016]	- 0.022 [- 0.027; - 0.018]	
AneuDepth *	0.031 [0.021; 0.04]	- 0.025 [- 0.033; - 0.017]	- 0.332 [- 0.349; - 0.315]	- 0.136 [- 0.154; - 0.118]	
Location_MCA +	0.933 [0.898; 0.968]	0.037 [0.026; 0.048]	0.852 [0.826; 0.879]	0.11 [0.094; 0.126]	
Location_PCOM +	1.107 [1.074; 1.141]	0.088 [0.075; 0.102]	0.904 [0.88; 0.927]	0.203 [0.18; 0.226]	
EarlierSAH_Yes +	0.421 [0.362; 0.479]	0.001 [- 0.004; 0.007]	0.326 [0.28; 0.371]	0.022 [0.009; 0.035]	
Hypertension_Yes-	- 0.73 [- 0.749; - 0.71]	- 0.084 [- 0.095; - 0.074]	- 0.569 [- 0.586; - 0.553]	- 0.155 [- 0.169; - 0.14]	
NWidth +			0.284 [0.272; 0.295]	0.189 [0.164; 0.214]	0.132 [0.113; 0.151]
NSI +			0.707 [0.695; 0.72]	0.248 [0.23; 0.266]	0.214 [0.2; 0.229]
Vol -			- 0.162 [- 0.18; - 0.143]	- 0.123 [- 0.136; - 0.109]	- 0.148 [- 0.169; - 0.126]
AbsHighPAreaPeak -		- 0.143 [- 0.155; - 0.13]		- 0.281 [- 0.305; - 0.256]	- 0.255 [- 0.279; - 0.231]
AbsHighWSSAreaPeak -		- 0.017 [- 0.02; - 0.014]		- 0.058 [- 0.066; - 0.05]	- 0.052 [- 0.059; - 0.044]
AbsHighWSSAreaAvg -		- 0.079 [- 0.087; - 0.071]		- 0.17 [- 0.185; - 0.155]	- 0.164 [- 0.18; - 0.148]
AbsLowWSSAreaAvg +		0.082 [0.073; 0.09]		0.157 [0.143; 0.171]	0.144 [0.128; 0.161]
AvgVPeak -		- 0.023 [- 0.027; - 0.018]		- 0.029 [- 0.039; - 0.02]	- 0.022 [- 0.031; - 0.012]
MaxOSI +		0.163 [0.15; 0.175]		0.24 [0.226; 0.254]	0.22 [0.206; 0.233]
MaxPPeak -		- 0.01 [- 0.014; - 0.005]		- 0.027 [- 0.035; - 0.018]	- 0.017 [- 0.026; - 0.009]
MaxVPeak +		0.046 [0.041; 0.052]		0.057 [0.048; 0.066]	0.044 [0.034; 0.054]
RelHighOSIArea +		0.053 [0.049; 0.056]		0.066 [0.058; 0.074]	0.088 [0.078; 0.097]
RelHighPAreaPeak -		- 0.086 [- 0.092; - 0.081]		- 0.05 [- 0.06; - 0.04]	- 0.045 [- 0.056; - 0.035]
RelHighWSSPeak -		- 0.055 [- 0.06; - 0.05]		- 0.023 [- 0.029; - 0.016]	- 0.014 [- 0.021; - 0.006]
RelLowWSSAreaAvg *		0.023 [0.017; 0.029]		- 0.018 [- 0.03; - 0.007]	- 0.021 [- 0.034; - 0.007]
RelInfluxAreaPeak -		- 0.078		- 0.098	- 0.112

Table 5 (continued)

Feature	P	PC	PS	PCS	CS
VisDis +		[- 0.081; - 0.074] 0.064 [0.052; 0.076]		[- 0.104; - 0.093] 0.166 [0.142; 0.19]	[- 0.118; - 0.106] 0.152 [0.129; 0.175]
Intercept -	- 0.513 [- 0.534; - 0.492]	- 0.025 [- 0.032; - 0.019]	- 0.451 [- 0.467; - 0.436]	- 0.078 [- 0.089; - 0.066]	- 0.02 [- 0.023; - 0.018]

The table contains only the variables that are retained in the models after the feature reduction stage. Positive coefficients mean that the feature is associated with rupture status and are marked with a plus sign (+). Negative coefficients mean that the feature is associated with unruptured status and are marked with a minus sign (-). Features that are associated with ruptured or unruptured status depending on the group in which they are included are marked with an asterisk (*). Bold coefficients indicate that the confidence interval includes the origin

(variables AbsHighWSSAreaPeak, AbsLowWSSAreaAvg), high values of velocity inside the aneurysm region and high viscous dissipation. Large high-pressure areas and volumes are indicative of unruptured aneurysms.

In accordance with what was observed before, the PCA-derived models show that haemodynamic or morphological data improve the predictive power of the logistic regression models. As PCA features are not interpretable and do not bear clinical relevance, their coefficients are not reported in the manuscript.

Discussion

This study assessed five logistic regression models constructed from different combinations of clinical, morphological (shape), and haemodynamic data for classifying aneurysms' rupture status. Previous studies have identified several morphological and haemodynamic factors which show statistical association with aneurysm rupture, and have shown that they can be used to classify ruptured and unruptured cases [7, 14, and 26]. However, they have not assessed whether the addition of these can improve established risk prediction models with respect to clinically established protocols. Our results show that, when compared to the PHASES score alone, the addition of either morphological or haemodynamic data individually improved classification accuracy. The addition of both morphological and haemodynamic data did not cause any further improvement.

Throughout our study, we also showed how through statistical approaches on a relatively large dataset we can reduce the number of image-derived features to those that demonstrate strongest association. This has been extensively debated through the scientific community [27–29], which recognises the importance of using robust statistical approaches and considerations when evaluating new potential image-derived features. This helps to avoid the proliferation of potentially confounding and misleading features, often arising from small, single-centre studies with

limited populations. Such features may lack statistical significance and hinder generalisability of results.

Our results show that haemodynamic analysis can effectively improve the separation between ruptured and unruptured cases. We have found that high OSI and low WSS are indicative of rupture, which is in accordance with previous observations [9, 26, and 30]. In the final set of retained variables, WSS does not directly appear through its values, but rather in terms of the area of the region where its values are high or low. This derives from the feature-reduction stage of the analysis, where we observed that MaxWSSPeak showed a high correlation ($r = 0.88$, $r < 0.001$) with MaxVPeak and was thus removed from the pool. The extension of aneurysm surface area exposed to low WSS (AbsLowWSSAreaAvg) is positively associated with rupture. This implies that, in case of rupture, large parts of the aneurysm are exposed to low WSS, a condition that has been identified as responsible for initiation, growth and rupture because of their role in endothelial remodelling [10, 31]. The association of WSS with rupture, however, is controversial and there exist studies that have linked rupture with high WSS [32]. This inconsistency can be partially explained by the observations in [33], where the authors hypothesised that aneurysms of different size fail because of various combinations of high/low WSS and oscillatory shear index (OSI). The OSI is a quantity derived from WSS that quantifies the oscillatory behaviour of the WSS vector along the cardiac cycle [34]. High OSI values are indicative of complex and dynamic flow patterns, vortices and recirculation regions within the aneurysm which ultimately induce low WSS and lower residence time [35]. Our models identify these conditions as associated with rupture status, coherently with results reported in [9, 36].

Complex haemodynamics is often induced by irregular shapes and geometries. NSI and AR are generally recognised as aggregated metrics for describing aneurysms' shape, with higher values describing shapes that differ from an ideal sphere [12, 37]. Deviations from spherical shape yield uneven distributions of wall stress which enhance aneurysm instability and favour rupture [12]. NSI higher than 0.2 have shown

significant discriminatory power in multiple studies [12, 37]. Our cohort of ruptured patients presented $NSI = 0.198 \pm 0.07$, and that feature ranked as highly influential in our analysis. AR was part of the initial set of variables but, despite being widely acknowledged as a risk factor for aneurysm rupture [12, 37], it was excluded from the final analysis. This was because of its correlation with the PHASES variable AneuDepth ($r = 0.79$, $p < 0.001$) and, by design, we decided to retain all the PHASES variables. Studies [5, 38] observed that patients with ruptured aneurysms showed higher values of AneuDepth. This association is confirmed in our analysis when only the PHASES variables are used as predictors but show an opposite direction when derived data are included. Previous studies [39, 40] have shown that narrow necks and larger volumes can induce blood stagnation within the aneurysm, thus creating haemodynamic conditions favourable for rupture. We did not observe this phenomenon in our results, and we ascribe it to the features of our cohort, where patients with large volumes and narrow necks tend to belong to the unruptured group. Other researchers have reported conclusions similar to ours [15, 41].

Despite this study showing the improved classification of aneurysm rupture with the addition of CFD and morphological derived factors, there remain several limitations. In terms of the CFD, the boundary conditions were obtained from generic 1D models of the brain circulations, while personalised models might offer a more precise representation of the boundary conditions. In terms of modelling, we did not include in our analysis variables derived from patients' lifestyle such as smoking and diet, or related to familial history of ruptured aneurysms and other cardiovascular pathologies. These are very well-established risk factors and regularly taken into consideration by doctors when evaluating possible treatment strategies [42]. However, they are not included among the PHASES variables and, since our study aims at evaluating the potential of CFD and shape analysis alongside the use of PHASES variables, we ultimately decided to exclude them from our model.

In terms of the population, our study is similar to previous studies [10, 26], and suffers from limited sample size and the cross-sectional nature of the dataset. The cross-sectional design of this study can explain a number of findings. It is not clear what is the effect of rupture on aneurysm shape and volume. Some authors report increases or while others report no modification [43, 44] in small-cohort studies. Our models identify smaller aneurysms (both in terms of Vol and AneuDepth) as predictive of unruptured status: however, without longitudinal observations to track their evolution, it is not possible to reach definitive conclusions on their role. Additionally, age showed an ambiguous effect in our models with elderly patients being more likely to rupture when exclusively considering the PHASES features, and less

prone to rupture when shape and haemodynamics are taken into account. While there are conflicting views regarding the role of age [45], elderly patients are more likely to have a diagnosis of an UIA and this will influence the structure of a dataset. Regarding hypertension, it was not associated with rupture. Our dataset did not include any actual blood pressure values, however. It is therefore possible that more patients with ruptured aneurysms had undiagnosed hypertension, whereas more patients with unruptured aneurysms had their blood pressure controlled on antihypertensive agents. Furthermore, only 27% of the patients in the ruptured group suffered from hypertension, which likely introduced a bias. Our dataset also included a similar number of ruptured and unruptured cases and did not represent the distribution of aneurysms in the general populations. This is an issue common to most currently available studies [10, 13, 15]. The dataset was also cross sectional and was used to develop a classifier capable of distinguishing someone with a ruptured aneurysm from someone with an unruptured aneurysm. The dataset did not allow us to assess if it could predict which unruptured aneurysms would go on to rupture in the future, which is the clinical question that needs to be addressed and what PHASES was developed for. Practically compiling the necessary longitudinal datasets to answer this question is challenging, however, due to the relatively low short rates of rupture, which mean very large datasets with very long periods of follow up are necessary. This is now being addressed in the Risk of Aneurysm Rupture (ROAR) study which is following up the largest cohort of patients with unruptured aneurysms to date with more than double the cases of the whole PHASES meta-analysis combined and far longer periods of follow up available [46]. Finally, our model was only validated internally, and we did not perform external validation. This is common to most computational studies [14–16, 21, 24], with the notable exception of [47]. The dataset used in this study, however, were collected during the @neurIST project which, despite being a large multicentric effort involving twenty-nine partners from twelve countries, did not have a uniformed data collection protocol. This implicitly guarantees that our model is robust to various images modalities. The size of the dataset we used, 170 patients, did not allow for further subdivisions based on the hospitals, while at the same time maintaining a meaningful sample size. Further validation of this model can be performed by resorting, for example, to larger datasets such as AneuX [48].

In conclusion, we showed that using additional data derived from CFD and morphological analysis increases the ability of logistic regression models in separating ruptured aneurysms from unruptured ones using clinical variables alone. The resulting logistic regression models achieved $AUC = 0.71$ and used a reduced number of features which

were obtained through semi-automated processing of medical images and CFD results. This approach has the potential to be included within current clinical protocols, once being extended and validated using longitudinal data and larger patient cohorts.

Supplementary Information The online version contains supplementary material available at <https://doi.org/10.1007/s11548-024-03289-7>.

Funding This research has received funding from the European Union (@neurIST project, Grant agreement: 027703; VPH-Share project, Grant agreement: 269978) and the UK EPSRC (CompBioMedX project, Project ID: EP/X019446/1).

Data availability Restrictions apply to the availability of patients' data, either clinical or derived from computational fluid dynamics and shape analysis and are not publicly available. Contact IB (i.benemerito@sheffield.ac.uk) for collaboration requests.

Declarations

Conflict of interest The authors declare no competing interests to disclose.

Ethical approval The project has received appropriate ethical approval for the required research. The ethical matters were managed by @neurIST Project Ethical Committee, Oxford, UK (Oxfordshire Research Ethics Committee-A Study Number: 07/Q1604/53).

Open Access This article is licensed under a Creative Commons Attribution 4.0 International License, which permits use, sharing, adaptation, distribution and reproduction in any medium or format, as long as you give appropriate credit to the original author(s) and the source, provide a link to the Creative Commons licence, and indicate if changes were made. The images or other third party material in this article are included in the article's Creative Commons licence, unless indicated otherwise in a credit line to the material. If material is not included in the article's Creative Commons licence and your intended use is not permitted by statutory regulation or exceeds the permitted use, you will need to obtain permission directly from the copyright holder. To view a copy of this licence, visit <http://creativecommons.org/licenses/by/4.0/>.

References

- Thompson BG, Brown RD Jr, Amin-Hanjani S, Broderick JP, Cockcroft KM, Connolly ES Jr, Duckwiler GR, Harris CC, Howard VJ, Johnston SC (2015) Guidelines for the management of patients with unruptured intracranial aneurysms: a guideline for healthcare professionals from the American heart association/american stroke association. *Stroke* 46(8):2368–2400
- Tawk RG, Hasan TF, D'Souza CE, Peel JB, Freeman WD (2021) Diagnosis and treatment of unruptured intracranial aneurysms and aneurysmal subarachnoid hemorrhage. *Mayo Clin Proc* 96(7):1970–2000. <https://doi.org/10.1016/j.mayocp.2021.01.005>
- Algra AM, Lindgren A, Vergouwen MDI, Greving JP, van der Schaaf IC, van Doormaal TPC, Rinkel GJE (2019) Procedural clinical complications, case-fatality risks, and risk factors in endovascular and neurosurgical treatment of unruptured intracranial aneurysms: a systematic review and meta-analysis. *JAMA Neurol* 76(3):282–293
- Naggara ON, Lecler A, Oppenheim C, Meder J-F, Raymond J (2012) Endovascular treatment of intracranial unruptured aneurysms: a systematic review of the literature on safety with emphasis on subgroup analyses. *Radiology* 263(3):828–835
- Greving JP, Wermer MJH, Brown RD, Morita A, Juvela S, Yonekura M, Ishibashi T, Torner JC, Nakayama T, Rinkel GJE (2014) Development of the PHASES score for prediction of risk of rupture of intracranial aneurysms: a pooled analysis of six prospective cohort studies. *Lancet Neurol* 13(1):59–66
- Bijlenga P, Gondar R, Schilling S, Morel S, Hirsch S, Cuony J, Corniola M-V, Perren F, Rüfenacht D, Schaller K (2017) PHASES score for the management of intracranial aneurysm: a cross-sectional population-based retrospective study. *Stroke* 48(8):2105–2112
- Feng X, Tong X, Chen J, Peng F, Niu H, Xia J, He X, Qi P, Lu J, Zhao Y (2021) External validation of the PHASES score in patients with multiple intracranial aneurysms. *J Stroke Cerebrovasc Dis* 30(5):105643
- Pagiola I, Mihalea C, Caroff J, Ikka L, Chalumeau V, Iacobucci M, Ozanne A, Gallas S, Marques M, Nalli D (2020) The PHASES score: to treat or not to treat? Retrospective evaluation of the risk of rupture of intracranial aneurysms in patients with aneurysmal subarachnoid hemorrhage. *J Neuroradiol* 47(5):349–352
- Zhou G, Zhu Y, Yin Y, Su M, Li M (2017) Association of wall shear stress with intracranial aneurysm rupture: systematic review and meta-analysis. *Sci Rep* 7(1):5331
- Tanioka S, Ishida F, Yamamoto A, Shimizu S, Sakaida H, Toyoda M, Kashiwagi N, Suzuki H (2020) Machine learning classification of cerebral aneurysm rupture status with morphologic variables and hemodynamic parameters. *Radiol: Artif Intell* 2(1):e190077. <https://doi.org/10.1148/ryai.2019190077>
- Li Y, Amili O, Moen S, Van de Moortele P-F, Grande A, Jagadeesan B, Coletti F (2022) Flow residence time in intracranial aneurysms evaluated by in vitro 4D flow MRI. *J Biomech* 141:111211
- Raghavan ML, Ma B, Harbaugh RE (2005) Quantified aneurysm shape and rupture risk. *J Neurosurg* 102(2):355–362
- Abi-Aad KR, Rahme RJ, Syal A, Nicole M, Turcotte EL, Patra DP, Jones B, Chong B, Krishna C, Bendok BR (2023) Predictive model evaluating risk of hemorrhage in intracranial aneurysms: analysis from prospectively collected HEAT trial database. *World neurosurg* 178:e315–e322
- Detmer FJ, Chung BJ, Jimenez C, Hamzei-Sichani F, Kallmes D, Putman C, Cebal JR (2019) Associations of hemodynamics, morphology, and patient characteristics with aneurysm rupture stratified by aneurysm location. *Neuroradiology* 61:275–284
- Detmer FJ, Chung BJ, Mut F, Slawski M, Hamzei-Sichani F, Putman C, Jiménez C, Cebal JR (2018) Development and internal validation of an aneurysm rupture probability model based on patient characteristics and aneurysm location, morphology, and hemodynamics. *Int J Comput Assist Radiol Surg* 13:1767–1779
- Ou C, Liu J, Qian Y, Chong W, Zhang X, Liu W, Su H, Zhang N, Zhang J, Duan C-Z (2020) Rupture risk assessment for cerebral aneurysm using interpretable machine learning on multidimensional data. *Front Neurol* 11:570181
- Shi Z, Hu B, Schoepf UJ, Savage RH, Dargis DM, Pan CW, Li XL, Ni QQ, Lu GM, Zhang LJ (2020) Artificial intelligence in the management of intracranial aneurysms: current status and future perspectives. *Am J Neuroradiol* 41(3):373–379
- Boeker M, Stenzhorn H, Kumpf K, Bijlenga P, Schulz S, Hanser S (2007) The @neurIST ontology of intracranial aneurysms: providing terminological services for an integrated IT infrastructure. In AMIA annual symposium proceedings. vol. 2007 No.: American Medical Informatics Association
- Villa-Uriol MC, Berti G, Hose DR, Marzo A, Chiarini A, Penrose J, Pozo J, Schmidt JG, Singh P, Lycett R (2011) @neurIST complex information processing toolchain for the integrated management of cerebral aneurysms. *Interface Focus* 1(3):308–319

20. Reymond P, Merenda F, Perren F, Rufenacht D, Stergiopoulos N (2009) Validation of a one-dimensional model of the systemic arterial tree. *Am J Physiol-Heart Circulatory Physiol* 297(1):H208–H222
21. Detmer FJ, Chung BJ, Mut F, Pritz M, Slawski M, Hamzei-Sichani F, Kallmes D, Putman C, Jimenez C, Cebal JR (2018) Development of a statistical model for discrimination of rupture status in posterior communicating artery aneurysms. *Acta Neurochir* 160:1643–1652
22. Venkatesh B, Anuradha J (2019) A review of feature selection and its methods. *Cybern Inf Technol* 19(1):3–26
23. Mwangi B, Tian TS, Soares JC (2014) A review of feature reduction techniques in neuroimaging. *Neuroinformatics* 12:229–244
24. Liu Q, Jiang P, Jiang Y, Ge H, Li S, Jin H, Li Y (2019) Prediction of aneurysm stability using a machine learning model based on PyRadiomics-derived morphological features. *Stroke* 50(9):2314–2321
25. Pedregosa F, Varoquaux G, Gramfort A, Michel V, Thirion B, Grisel O, Blondel M, Prettenhofer P, Weiss R, Dubourg V (2011) Scikit-learn: machine learning in Python. *J Mach Learn Res* 12:2825–2830
26. Xiang J, Natarajan SK, Tremmel M, Ma D, Mocco J, Hopkins LN, Siddiqui AH, Levy EI, Meng H (2011) Hemodynamic–morphologic discriminants for intracranial aneurysm rupture. *Stroke* 42(1):144–152
27. Kallmes D.F (2012) Point: CFD—computational fluid dynamics or confounding factor dissemination. *AJNR: Am J Neuroradiol* 33(3): 395
28. Cebal JR, Meng H (2012) Counterpoint: realizing the clinical utility of computational fluid dynamics—closing the gap. *Am J Neuroradiol* 33(3):396–398. <https://doi.org/10.3174/ajnr.A2994>
29. Robertson AM, Watton PN (2012) Computational fluid dynamics in aneurysm research: critical reflections, future directions. *Am J Neuroradiol* 33(6):992–995. <https://doi.org/10.3174/ajnr.A3192>
30. Lv N, Karmonik C, Chen S, Wang X, Fang Y, Huang Q, Liu J (2020) Wall enhancement, hemodynamics, and morphology in unruptured intracranial aneurysms with high rupture risk. *Transl Stroke Res* 11:882–889
31. Bousset L, Rayz V, McCulloch C, Martin A, Acevedo-Bolton G, Lawton M, Higashida R, Smith WS, Young WL, Saloner D (2008) Aneurysm growth occurs at region of low wall shear stress: patient-specific correlation of hemodynamics and growth in a longitudinal study. *Stroke* 39(11):2997–3002
32. Meng H, Wang Z, Hoi Y, Gao L, Metaxa E, Swartz DD, Kolega J (2007) Complex hemodynamics at the apex of an arterial bifurcation induces vascular remodeling resembling cerebral aneurysm initiation. *Stroke* 38(6):1924–1931
33. Meng H, Tutino VM, Xiang J, Siddiqui A (2014) High WSS or low WSS? Complex interactions of hemodynamics with intracranial aneurysm initiation, growth, and rupture: toward a unifying hypothesis. *Am J Neuroradiol* 35(7):1254–1262
34. Sheikh MAA, Shuib AS, Mohyi MHH (2020) A review of hemodynamic parameters in cerebral aneurysm. *Interdisciplinary Neurosurg* 22:100716
35. Ryu C-W, Kwon OK, Koh JS, Kim EJ (2011) Analysis of aneurysm rupture in relation to the geometric indices: aspect ratio, volume, and volume-to-neck ratio. *Neuroradiology* 53:883–889
36. Shojima M, Oshima M, Takagi K, Torii R, Hayakawa M, Katada K, Morita A, Kirino T (2004) Magnitude and role of wall shear stress on cerebral aneurysm: computational fluid dynamic study of 20 middle cerebral artery aneurysms. *Stroke* 35(11):2500–2505
37. Sanchez S, Hickerson M, Patel RR, Ghazaleh D, Tarchand R, Paranjape GS, Pope H, Ortega-Gutierrez S, Pederson JM, Hasan D (2023) Morphological characteristics of ruptured brain aneurysms: a systematic literature review and meta-analysis. *Stroke: Vasc Inter-ventional Neurol* 3(2):e000707
38. Waqas M, Chin F, Rajabzadeh-Oghaz H, Gong AD, Rai HH, Mokin M, Vakharia K, Dossani RH, Meng H, Snyder KV (2020) Size of ruptured intracranial aneurysms: a systematic review and meta-analysis. *Acta Neurochir* 162:1353–1362
39. Ujiie H, Tachibana H, Hiramatsu O, Hazel AL, Matsumoto T, Ogasawara Y, Nakajima H, Hori T, Takakura K, Kajiya F (1999) Effects of size and shape (aspect ratio) on the hemodynamics of saccular aneurysms: a possible index for surgical treatment of intracranial aneurysms. *Neurosurgery* 45(1):119
40. Kleinloog R, De Mul N, Verweij BH, Post JA, Rinkel GJE, Ruigrok YM (2018) Risk factors for intracranial aneurysm rupture: a systematic review. *Neurosurgery* 82(4):431–440
41. Dhar S, Tremmel M, Mocco J, Kim M, Yamamoto J, Siddiqui AH, Hopkins LN, Meng H (2008) Morphology parameters for intracranial aneurysm rupture risk assessment. *Neurosurgery* 63(2):185–197
42. Bandhauer B, Gruber P, Anderegg L, Berberat J, Wanderer S, Cattaneo M, Schubert GA, Remonda L, Marbacher S, Grüter BE (2024) From conservative to interventional management in unruptured intracranial aneurysms. *J Neurosurg* 1:1–7
43. Yi J, Zielinski D, Chen M (2016) Cerebral aneurysm size before and after rupture: case series and literature review. *J Stroke Cerebrovasc Dis* 25(5):1244–1248
44. Schneiders JJ, Marquering HA, Van den Berg R, VanBavel E, Velthuis B, Rinkel GJE, Majoie CB (2014) Rupture-associated changes of cerebral aneurysm geometry: high-resolution 3D imaging before and after rupture. *Am J Neuroradiol* 35(7):1358–1362
45. Backes D, Rinkel GJE, Laban KG, Algra A, Vergouwen MDI (2016) Patient-and aneurysm-specific risk factors for intracranial aneurysm growth: a systematic review and meta-analysis. *Stroke* 47(4):951–957
46. Hall S, Birks J, Anderson I, Bacon A, Brennan PM, Bennett D, Chavredakis E, Critchley G, Dow G, Downer J (2023) Risk of aneurysm rupture (ROAR) study: protocol for a long-term, longitudinal, UK multicentre study of unruptured intracranial aneurysms. *BMJ Open* 13(3):e070504
47. Detmer FJ, Fajardo-Jiménez D, Mut F, Juchler N, Hirsch S, Pereira VM, Bijlenga P, Cebal JR (2018) External validation of cerebral aneurysm rupture probability model with data from two patient cohorts. *Acta Neurochir* 160:2425–2434
48. Juchler N, Schilling S, Bijlenga P, Kurtcuoglu V, Hirsch S (2022) Shape trumps size: image-based morphological analysis reveals that the 3D shape discriminates intracranial aneurysm disease status better than aneurysm size. *Front Neurol* 13:809391

Publisher's Note Springer Nature remains neutral with regard to jurisdictional claims in published maps and institutional affiliations.